

Substitutional carbon in group-III nitrides: *Ab initio* description of shallow and deep levelsL.E. Ramos,^{1,2} J. Furthmüller,¹ L.M.R. Scolfaro,² J.R. Leite,² and F. Bechstedt¹¹*Institut für Festkörperteorie und Theoretische Optik, Friedrich-Schiller-Universität, 07743 Jena, Germany*²*Universidade de São Paulo, Instituto de Física, CP66318, 05315-970 São Paulo SP, Brazil*

(Received 01 March 2002; revised manuscript received 30 April 2002; published 26 August 2002)

We present *ab initio* pseudopotential plane-wave calculations for the neutral and negatively charged carbon impurity on a nitrogen site in group-III nitrides. Ultrasoft non-norm-conserving Vanderbilt pseudopotentials allow the use of extremely large supercells up to 2744 atoms. These supercells attenuate the defect-defect interaction and, hence, give an accurate description of the resulting acceptor levels in BN, AlN, GaN, and InN. We calculate atomic geometries and energetical positions of the defect levels, Franck-Condon shifts, and formation energies. The defect stability and the transition of the shallow-deep character are discussed along the series BN, AlN, GaN, and InN. For GaN we calculate a hole activation energy of about 0.2 eV in correspondence with photoluminescence and temperature-dependent Hall measurements.

DOI: 10.1103/PhysRevB.66.075209

PACS number(s): 61.72.Bb, 61.72.Vv, 71.55.Eq

I. INTRODUCTION

Group-III nitrides are materials of considerable interest in electronic and optoelectronic devices due to their high thermal and mechanical stabilities, the formation of alloy systems and, hence, the possibility of band-gap engineering.¹ Optical and electrical properties of semiconductors are mainly controlled by point defects such as vacancies, antisites, and intentional and unintentional impurities. For the development of devices reliable information about point defects and techniques to control the doping process are crucial. Carbon is an unintentional impurity appearing during the growth of group-III nitrides.^{2–6} However, the role of carbon in these materials is controversial. The ionic radii indicate that C should have a nonvanishing solubility in the cation sublattices, in particular in the Ga and Al sublattices.¹ Due to its small ionic radius, carbon fits in the nitrogen site. Indeed, theoretical predictions found that in GaN the incorporation of C on a N site should be preferred.⁷ In this nitride, magnesium is the most common impurity to achieve *p*-type conductivity, giving rise to relatively low hole concentrations and a high acceptor ionization level at room temperature.⁸ However, there are indications that high *p*-type carrier concentrations can be achieved using carbon as a dopant material in GaN.⁹ Recent experimental results suggested carbon in the nitrogen site (C_N) as an alternative to Mg in cubic (*c*) GaN.¹⁰ Compensation effects supposedly caused by defect complexes such as carbon pairs discouraged its use as a *p*-type impurity in wurtzite (*w*) GaN.¹¹

The group-III nitrides AlN, GaN, and InN crystallize in the hexagonal wurtzite phase¹² under ambient conditions. However, these nitrides can also be grown in a cubic zincblende phase which offers, in principle, many advantages with relation to the wurtzite phase, such as a higher crystal symmetry, higher carrier mobility due to a smaller scattering coefficient, lower effective masses, and easy cleavage.¹³ Cubic BN crystals were first synthesized in 1957 by Wentfort,¹⁴ and with the use of certain techniques¹⁵ high-quality samples large enough to be characterized can be achieved. The growth of *c*-AlN was first reported by Petrov *et al.*,¹⁶ and additional techniques have improved the quality and size of

the crystals obtained.⁶ Zinc-blende GaN is commonly grown by molecular-beam epitaxy.¹⁷ Although *c*-InN is the least studied nitride, thick layers of this material were synthesized and characterized recently.¹⁸ Since the structural differences between the wurtzite and cubic phases refer to second neighbors, it is useful to study the doping behavior of an impurity in the zinc-blende phase.

Using a tight-binding version of the linear muffin-tin orbital (LMTO) method in the atomic sphere approximation (ASA), 64-atom supercells, and relaxation of the atomic positions, Gubanov *et al.*¹⁹ found that C_N in *c*-BN gives rise to a shallow single-particle acceptor level. Similar results were obtained with the full-potential linear augmented plane wave method without relaxation and with the same supercell size.²⁰ Within the frameworks of the density-functional theory (DFT) formalism and the generalized-gradient approximation, normconserving pseudopotentials and relaxation of atomic forces, Orellana and Chacham²¹ considered additional positively charged states and speculated about a negative-*U* behavior for C_N in BN. Comprehensive calculations of the carbon impurity in AlN, GaN, and InN by Jenkins and Dow, including their alloys in the wurtzite phase, were based on an empirical treatment within the tight-binding approximation.²² Very shallow single-particle levels or even levels resonant to the valence band were obtained for C_N in AlN and GaN, whereas for InN a deeper level was predicted. Later calculations for *w*-GaN using normconserving pseudopotentials and the DFT in the local-density approximation (LDA) predicted a shallow acceptor level for C_N . Neugebauer and Van de Walle⁷ discussed carbon as the origin of the parasitic yellow luminescence observed in this compound. Calculations to determine the doping properties of carbon in *w*-AlN and *w*-GaN were performed by Boguslawski and co-workers^{23,24} applying quantum molecular dynamics and the pseudopotential formalism. The properties of the neutral carbon impurity in cubic BN, AlN, and GaN were also investigated by Gorczyca *et al.*²⁵ using a combination of LMTO-ASA Green's function methods. A full-potential version of the LMTO code was applied to perform the relaxation of the atomic positions.^{26,27} Theoretical studies of impurities in InN are scarce. Within the DFT-LDA, most

of the methods give rise to a negative fundamental gap for *c*-InN, even if more sophisticated all-electron methods are applied.²⁸ Stampfl *et al.*²⁹ studied O, Si, and Mg impurities in *c*-InN using self-interaction and relaxation-corrected pseudopotentials which helped to solve the problem of the negative fundamental gap. However, they concluded that the results are qualitatively the same as within the usual DFT-LDA pseudopotential plane-wave methods.

The *ab initio* calculations up to now refer to isolated carbon impurity in small supercells with 32–72 atoms. The size of the supercell used may influence the results at least for two reasons. First, the interaction between the defect and its images in the neighboring cells may play an important role. For the charged impurity, Coulomb interaction effects resulting from the defect-defect interaction are inversely proportional to a linear dimension or edge length L of the supercell. To account for these, some corrections to the total energy may be used as proposed in the literature.^{30,31} Second, the supercell size should be more critical in cases where C_N gives rise to shallow levels. The accompanying wave functions are extended, and the supercell size should be larger than their localization radii to avoid an artificial spatial quantization.

Although the computational effort may increase as much as L^3 , the simplest way to suppress the defect-defect interaction is to increase the supercell size. In the present paper, we therefore increase the supercell size substantially to reduce the spurious interactions. The convergence with respect to the supercell size is studied for the position of the single-particle Kohn-Sham (KS) levels, the ionization levels, and the formation energies. Other quantities that can be estimated by the delta-self-consistent-field method (Δ SCF), such as relaxation energy and Franck-Condon shifts are also examined. The paper is organized as follows. In Sec. II, we describe the methods used for the calculation of the total energy, the Kohn-Sham defect levels, the formation energies and ionization levels for the carbon impurity. The results are discussed in Sec. III, and in Sec. IV a brief summary is given.

II. METHOD

A. Total-energy calculations

The total-energy calculations are based on DFT (Ref. 32) in the LDA or the local spin-density approximation (Ref. 33). Quantum Monte Carlo results in the parametrization of Perdew and Zunger³⁴ are used to describe the exchange-correlation energy. The correlation energy for an arbitrary spin polarization is determined by a standard interpolation³⁵ between the values of the nonpolarized and fully polarized cases. The valence electrons of B, Al, Ga, In, N, and C, as well as the d electrons of In and Ga, are treated explicitly. Their interaction with the atomic cores is taken into account by means of non-norm-conserving *ab initio* Vanderbilt pseudopotentials. They allow a considerable softening of the pseudopotentials of the first-row elements as well as of the atoms with filled d shells.³⁶ The energy cutoff for the plane-wave expansion of the single-particle eigenfunctions is restricted to 19.9 Ry (14.0, 16.2, and 15.5 Ry) for BN (AlN,

GaN, and InN). The atomic forces are calculated directly from the free-energy functional³⁷ of the system applying the Hellmann-Feynman (HF) theorem.³⁸ Explicitly we use the Vienna *ab initio* simulation package.³⁷ Monkhorst-Pack type meshes³⁹ in the irreducible part of the Brillouin zone are used to approximate the \mathbf{k} -space integrals. The calculations include the relaxation of the atomic positions around the impurity, in order to find the equilibrium atomic configuration for a certain charge state. The spin polarization is taken into account for the neutral C impurity.

For BN, AlN, GaN, and InN, we study the carbon impurity on the nitrogen site in simple cubic supercells with 64–2744 atoms and different \mathbf{k} -point meshes. Explicitly we use $2 \times 2 \times 2$ and $4 \times 4 \times 4$ \mathbf{k} -point meshes for the 64-atom supercells, and $2 \times 2 \times 2$ mesh for the 512-atom supercells. The self-consistent energy calculations are restricted only to the Γ point for the 1000-atom (BN and GaN), 1728-atom (AlN), and 2744-atom (BN) supercells. For the BN 1000-atom supercell we also applied a $2 \times 2 \times 2$ \mathbf{k} -point mesh to verify the applicability of the Γ -only calculations for the large supercells.

In 64-atom supercells the total energies do not change significantly (10–50 meV) when a $4 \times 4 \times 4$ mesh is applied instead of $2 \times 2 \times 2$ mesh for BN, AlN, and GaN. For BN in 1000-atom supercells, Γ -only and $2 \times 2 \times 2$ calculations lead to similar results for the KS defect levels and ionization levels, reinforcing the applicability of Γ -only calculations for large supercells. Total-energy calculations could be made for InN:C in 64-atom supercells, but correct identifications of the defect levels, the top of the valence band, and the bottom of the conduction band demand more states; therefore 512-atom supercells are considered.

The geometry of the fully relaxed structures and the HF forces acting on the atoms in the ideal zinc-blende crystal are determined for the first- (1nn) and second-nearest (2nn) neighbors. Orthonormal basis sets ($\mathbf{b}_{ij}, \mathbf{p}_{ij}, \mathbf{n}_{ij}$) are used to project the HF forces $\mathbf{F}_{ij}^{\text{HF}}$ and displacement vectors $\Delta \mathbf{d}_{ij}$. The displacements and forces on the four first neighbors ($i = 0, 1, 2, 3$) of the impurity site ($j = 0$) are described by means of sets of orthonormal basis ($\mathbf{b}_{i0}, \mathbf{p}_{i0}, \mathbf{n}_{i0}$),⁴⁰ where the breathing mode vectors \mathbf{b}_{i0} are along the lines connecting the carbon site to each first neighbor, the pairing mode vectors \mathbf{p}_{i0} are along the lines between two equivalent first neighbors, and the \mathbf{n}_{i0} vectors are orthogonal to both \mathbf{p}_{i0} and \mathbf{b}_{i0} . For the description of the displacements and forces at the 12 second neighbors ($i = 0, 1, 2, 3$ and $j = 1, 2, 3$) we apply different basis sets ($\mathbf{b}_{ij}, \mathbf{p}_{ij}, \mathbf{n}_{ij}$). In the case of the second neighbors, both components \mathbf{b}_{ij} and \mathbf{p}_{ij} point toward second-neighbor sites in the same plane and the components \mathbf{n}_{ij} are orthogonal to the others.

B. Formation energies and ionization levels

The formation energy for the carbon impurity on a substitutional N site in the binary compound XN ($X = \text{B, Al, Ga, and In}$) is calculated in the formalism of Zhang and Northrup⁴¹ by

$$\Omega_f(XN:C_N^q, E_F) = E_{tot}^Q(XN:C_N^q) - E_{tot}^{ideal}(XN) + \mu(N) - \mu(C) + qE_F, \quad (1)$$

where $E_{tot}^Q(XN:C_N^q)$ is the total energy of the XN supercell with a C atom in the charge state q . Q indicates the charge state in whose geometry the total energy is calculated. $Q \neq q$ means a total energy from a calculation for the charge state q in the geometry of the charge state Q . $E_{tot}^q(XN:C_N^q)$ gives the minimum total energy for the charge state q . $E_{tot}^{ideal}(XN)$ denotes the total energy of the corresponding ideal zinc-blende supercell of XN, $\mu(N)$ and $\mu(C)$ are the chemical potentials of N and C, respectively, for certain preparation conditions, and E_F is the Fermi level. The latter quantity is divided according to $E_F = E_V(XN) + \varepsilon_F$, where $E_V(XN)$ corresponds to the valence band maximum (VBM) of the host nitride and the reduced Fermi level ε_F varies from zero to the value of the fundamental gap E_{gap} of XN. For the fundamental energy gaps we applied the values of calculations reported in the literature including the quasiparticle corrections⁴²⁻⁴⁴ $E_{gap} = 6.3$ (BN), 4.9 (AlN), 3.1 (GaN), and 0.52 eV (InN). The underestimation of the gap values for GaN and InN is a consequence of the overestimation of the p - d orbital repulsion within the explicit treatment of the semicore d -electrons by DFT-LDA. The top of valence band $E_V(XN)$ is usually not well defined in a supercell calculation of systems with impurity. The electrostatic potential is different from the defect-free material and the shallow acceptor states influence the VBM. We therefore align the lowest occupied s -like valence states of supercell systems with and without impurity.

The chemical potentials of the carbon, $\mu(C)$, and nitrogen, $\mu(N)$, are determined using the standard procedure described in the literature.^{41,45} The upper limit for the carbon chemical potential in Eq. (1) is taken from a DFT-LDA calculation for the cohesive energy of its diamond structure. Since we are interested in the system where the carbon is more likely to be incorporated in the sample, we consider C-rich preparation conditions to calculate the formation energies.

In thermal equilibrium, the chemical potentials $\mu(N)$ and $\mu(X)$ depend linearly on each other because of the mass action law. They are related to the bulk chemical potential $\mu(XN_{bulk})$ of the binary compound XN. The difference between this quantity and the chemical potentials $\mu(X_{bulk})$ of the cation and $\mu(N_{bulk})$ of the nitrogen defines the heat of formation $\Delta H_f(XN)$ of the compound XN. The two relations allow the representation of the chemical potential of the nitrogen atoms in Eq. (1) by

$$\mu(N) = \mu(XN_{bulk}) - \mu(X_{bulk}) + \Delta H_f(XN) + \Delta\mu(N). \quad (2)$$

The fluctuation $\Delta\mu(N)$ of the N chemical potential varies between $\Delta\mu(N) = -\Delta H_f(XN)$ (X -rich preparation conditions) and $\Delta\mu(N) = 0$ (N-rich preparation conditions). To be consistent with the total energies of the supercells, we apply calculated values of $\mu(XN_{bulk})$ and $\mu(X_{bulk})$.⁴⁶ The heat of formation, estimated from measured quantities, leads to the

values $\Delta H_f(XN) = 2.65$ ($X = B$), 3.28 ($X = Al$), 1.28 ($X = Ga$), and 0.38 eV ($X = In$) per XN pair.

The position of the Fermi level at which the formation energy of an impurity in the different charged states q and $q+1$ becomes equal is called ionization level. According to Eq. (1) the ionization level is defined in the framework of the Δ SCF method by

$$\varepsilon(q+1/q) = E_{tot}^q(XN:C_N^q) - E_{tot}^{q+1}(XN:C_N^{q+1}) - E_V(XN), \quad (3)$$

where $E_V(XN)$ is the eigenvalue of the VBM from a bulk calculation. In the relevant case $q = 1 -$, the energy in Eq. (3) may be interpreted as the binding energy of a hole. It is assumed that for each charge state $q = 0, 1 -$ of the carbon impurity, the atomic configuration is that of fully-relaxed atomic positions. Therefore, the energy in Eq. (3) should be strongly related to the thermal activation energy of the holes since in this process the system has sufficient time to change into the geometry of a negatively charged state.

C. Franck-Condon shifts and lattice relaxation

Single and two-particle excitation energies of the type given in Eq. (3) correspond to differences between total energies. If one neglects the electron-hole pair binding, the ionization levels can be hence calculated not only in the single-particle case but also after two-particle excitation by a Δ SCF method. However, the two different total energies considered in the Δ SCF, $E_{tot}^Q(XN:C_N^q)$, do not only depend on the actual charge state q of the defect but also on the particular geometry that has been optimized for the charge state Q . For very fast transitions between two charge states q and $q+1$, the system has not enough time to relax the atomic positions and the energies have to be computed assuming the geometry of the charge state Q of the initial configuration.

The process of the hole excitation can be discussed in a energy-configurational coordinate diagram in which four points (a , b , c , and d) are considered. The points a and b correspond to the ground and excited state respectively in the fully relaxed geometry of C_N^0 , whereas the points c and d represent the latter states in the fully relaxed geometry of C_N^{1-} . The system is in the ground state at a and during an optical emission process, an electron is captured driving the system to the point b . Then the system relax into another minimum energy position at c , emitting phonons for instance. The point b is identified with the charged defect C_N^{1-} in the geometry of C_N^0 , whereas the point c matches the charged defect with fully-relaxed atomic positions. When an optical absorption process occurs, the system is driven to a point d which corresponds to the ground state C_N^0 in the geometry of the excited state C_N^{1-} . The energies of the transitions $a \rightarrow b$ and $c \rightarrow d$ can be extracted from optical measurements. For instance, in a photoluminescence (PL) experiment, optical transitions of the type $C_N^0 + e^- \rightarrow C_N^{1-}$ occur when an electron e^- in the conduction-band minimum is captured by the defect and the system remains still in the geometry of the neutral state. The binding energy of the electron and hole in the acceptor-bound exciton is thereby disre-

garded in a first approximation. The corresponding photon energy of emitted light is given by $\hbar\omega_E = E_{gap} - \varepsilon_E(0/1-)$ with an optical activation energy of the hole of

$$\varepsilon_E(0/1-) = E_{tot}^0(XN:C_N^{1-}) - E_{tot}^0(XN:C_N^0) - E_V(XN). \quad (4)$$

The absorption of a photon is accompanied by the generation of an electron-hole pair and the negatively charged defect becomes neutral, $C_N^{1-} \rightarrow C_N^0 + e^-$. Again neglecting the exciton binding energy, the excited electron occupies a state in the conduction band. The corresponding photon energy of absorption is $\hbar\omega_A = E_{gap} - \varepsilon_A(0/1-)$ with another activation energy

$$\varepsilon_A(0/1-) = E_{tot}^{1-}(XN:C_N^{1-}) - E_{tot}^{1-}(XN:C_N^0) - E_V(XN). \quad (5)$$

The difference between these two optical excitation energies defines the Franck-Condon (FC) shift⁴⁷

$$\begin{aligned} \Delta E_{FC}^{optical} &= \hbar(\omega_E - \omega_A) \\ &= \varepsilon_E(0/1-) - \varepsilon_A(0/1-) \\ &= E_{tot}^0(XN:C_N^{1-}) + E_{tot}^{1-}(XN:C_N^0) \\ &\quad - E_{tot}^0(XN:C_N^0) - E_{tot}^{1-}(XN:C_N^{1-}). \end{aligned} \quad (6)$$

PL and temperature-dependent Hall-effect measurements provide different values of activation energies⁸ for a given acceptor which corresponds to the electronic transitions between its neutral and excited states. These values of activation energies are related to the hole excitations during optical or thermal activation. In this case one can define the thermal FC shift

$$\begin{aligned} \Delta E_{FC}^{thermal} &= \varepsilon_E(0/1-) - \varepsilon(0/1-) \\ &= E_{tot}^0(XN:C_N^{1-}) - E_{tot}^{1-}(XN:C_N^{1-}). \end{aligned} \quad (7)$$

The FC shifts has been successfully calculated by *ab initio* methods for the Mg impurity in GaN.⁴⁸ These results indeed allow the explanation of the difference in the hole activation energies derived from PL and Hall measurements.

The different FC shifts are consequences of the different atomic geometries occurring around the carbon impurity C_N^q in different charged states Q . Characteristic energies for these relaxations may be calculated by the energy gain of the total energy due to the atomic displacements with respect to the atomic positions of an ideal zinc-blende lattice:

$$\Delta E(C_N^q) = E_{tot}^{ideal}(XN:C_N^q) - E_{tot}^q(XN:C_N^q). \quad (8)$$

These energy contributions can be approximated by the work done by the Hellmann-Feynman forces W_{nn}^{HF} along the path followed by the atoms during the successive steps of the relaxation. Since first and second neighbors to the carbon site are displaced according to the forces \mathbf{F}_{ij}^{HF} , they may experience different displacements $\Delta \mathbf{d}_{ij}$. Consequently, the different neighbors can contribute differently to the relaxation energy $\Delta E(C_N^q)$. For short displacements it is reasonable to

TABLE I. Displacements Δd (in percentage of the bond length d) and work of the HF forces W_{nn}^{HF} (in meV) for the first (1) and second (2) nearest neighbors as well as relaxation energies $\Delta E(C_N^q)$ (in meV).

Defect	Nitride		$\Delta d(\mathbf{b}_{ij})$	$\Delta d(\mathbf{n}_{ij})$	$\Delta E(C_N^q)$	W_{nn}^{HF}
C_N^0	BN	1	0.86	0.00	68	3
		2	1.07	-0.05		55
	AlN	1	2.87	0.00	146	101
		2	1.50	0.05		48
	GaN	1	-0.05	0.00	68	0.4
		2	1.25	0.11		58
	InN	1	-0.20	0.00	47	2
		2	1.11	0.28		39
C_N^{1-}	BN	1	-0.49	0.00	272	16
		2	1.33	0.00		131
	AlN	1	0.07	0.00	368	-2
		2	2.16	0.31		243
	GaN	1	-1.12	0.00	286	48
		2	1.62	0.22		152
	InN	1	-0.87	0.00	120	21
		2	1.23	0.32		67

approximate the force at each of the successive atomic positions by a constant value given by one-half of the force in the case of zinc-blende atomic positions. In order to estimate the different contributions to the energy relaxation due to the first- and second-nearest neighbors, we divide the main part of the lattice relaxation energy according to

$$W_{nn}^{HF} = \frac{1}{2} \sum_{i=0}^3 \mathbf{F}_{i0}^{HF} \Delta \mathbf{d}_{i0} + \frac{1}{2} \sum_{i=0, j=1}^3 \mathbf{F}_{ij}^{HF} \Delta \mathbf{d}_{ij}, \quad (9)$$

where the contribution due to the more distant neighbors is not taken into account. The result is compared to the value obtained by Eq. (8).

III. RESULTS

A. Lattice relaxation

Displacing the carbon atom slightly and arbitrarily from its zinc-blende position on the nitrogen sublattice and allowing the relaxation of all the host atoms, we verified that its final relaxed position is still the center of a tetrahedron formed by its first nearest-neighbor cations. Therefore, we do not find any indication of a symmetry-lowering Jahn-Teller distortion independent of the charge state of the impurity $q = 0, 1-$ and of the group-III nitride. For that reason only the T_d symmetry is discussed in the following. All the group-III nitrides show a breathing-mode relaxation on the nearest neighbors around the carbon impurity. The corresponding geometrical changes given in percentage of the bond length d are listed for the first- and second-nearest neighbors atoms in Table I. The results are obtained for converged spin-polarized calculations using relatively large supercells with 2744 (BN), 1728 (AlN), 1000 (GaN), and 512 (InN) atoms.

TABLE II. Franck-Condon shifts ($\Delta E_{\text{FC}}^{\text{optical}}$ and $\Delta E_{\text{FC}}^{\text{thermal}}$), Kohn-Sham eigenvalues of the t_2 defect level $\varepsilon_{t_2}(q=0)$ and $\varepsilon_{t_2}(q=1-)$ (including their spin up and down splitting for $q=0$), and acceptor ionization energies $\varepsilon(0/1-)$ (in meV). The Kohn-Sham eigenvalues are given with respect to the VBM.

Nitride	$\Delta E_{\text{FC}}^{\text{optical}}$	$\Delta E_{\text{FC}}^{\text{thermal}}$	$\varepsilon_{t_2}(q=0)$	$\varepsilon_{t_2}(q=1-)$	$\varepsilon(0/1-)$
BN	208	129	150	538	293
			83		
AlN	688	382	603	1178	867
			306		
GaN	140	89	116	288	182
			58		
InN	35	20	54	92	12
			33		

The charge state and the cation of the nitride determine the direction and strength of the breathing mode. The 2nn N atoms exhibit always remarkable outward breathing-mode displacements, which are accompanied by short displacements in the \mathbf{n}_{ij} direction. In GaN and InN, the 1nn cations are displaced inwards. The increase of these displacements with the number of electrons is a consequence of the formation of four strong bonds in the case of isoelectronic C_N^{1-} . The bonding effect is also responsible for the outward (inward) breathing relaxation in BN for $q=0$ ($q=1-$). No chemical trend along the row InN, GaN, AlN, and BN is observed. Only in large supercells, an outward breathing relaxation occurs for AlN which is small for $q=1-$ and takes the largest value for $q=0$.

In general, our predictions agree with the results of other authors with respect to the direction of the breathing relaxation. They also reported small relaxations for all the group-III nitrides of about 0.1–4.0% of the bond length for c -BN,^{20,21} AlN, and GaN,^{20,24,26} or even found that there is no relaxation for C_N^0 in BN and AlN.^{26,27} However we cannot confirm, even for small supercells, the prediction of an inward relaxation for BN in the neutral charge state.^{19,21}

The lattice relaxation can be characterized by means of the relaxation energies $\Delta E(\text{C}_\text{N}^q)$ defined in Eq. (8) and the FC shifts $\Delta E_{\text{FC}}^{\text{optical}}$ and $\Delta E_{\text{FC}}^{\text{thermal}}$ given in Eqs. (6) and (7), respectively. Their most converged values are presented in Tables I and II, and their behavior versus the edge length $L = (2/\sqrt{3})d(\text{number of atoms})^{1/3}$ of the supercells is plotted in Fig. 1. The relaxation energy for the neutral impurity is already converged for small supercells. Although for the negatively charged defect its value increases with increasing L , there is a compensation effect when the FC shifts are calculated. Indeed, for BN and GaN the FC shifts already reach converged values for small supercells. The relaxation energies in Table I show two opposite tendencies along the series InN, GaN, AlN, and BN. For the neutral impurity, the relaxation energy amounts to 50–70 meV for InN, GaN, and BN, and is approximately two times higher for AlN. For the negatively-charged state, the relaxation energies increase dramatically when the size of the supercell is increased. Nevertheless, in comparison with other authors who predicted

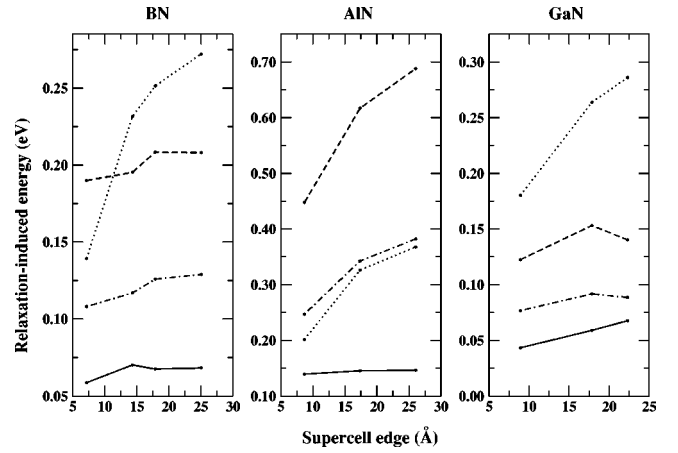


FIG. 1. Lattice relaxation energy $\Delta E(\text{C}_\text{N}^q)$ for the neutral (solid line) and negatively charged (dotted line) calculated Franck-Condon shifts $\Delta E_{\text{FC}}^{\text{optical}}$ (dashed line) and $\Delta E_{\text{FC}}^{\text{thermal}}$ (dot-dashed line) for the carbon impurity in BN, AlN, and GaN as a function of the supercell edge.

relaxation energies ranging from 0.1 to 0.9 eV (Refs. 21 and 24) for the carbon in the group-III nitrides, we find relatively low relaxation energies. The work of the Hellmann-Feynman forces W_{nn}^{HF} in Table I indicates that the mechanism of relaxation is governed by the 2nn atoms. The only exception is again C_N^0 in AlN, for which the 2.9% outward breathing-mode relaxation of the 1nn atoms is more important.

The optical and thermal Franck-Condon shifts in Table II show similar trends as the relaxation energies $\Delta E(\text{C}_\text{N}^q)$ in Table I. They are about three or four times larger for AlN than for BN and GaN. These higher values indicate a strong coupling with phonons in both $q=0$ and $1-$ cases for BN, AlN, and GaN, whereas the effect is remarkably reduced in InN. Interestingly, the shifts of the thermal activation energies amount to about 50–65% of the optical FC shifts measurable in PL and optical absorption experiments.

B. Defect levels

Information about the position of defect levels can be obtained either through the total energies from ΔSCF methods, i.e., including many-particle effects, or within the picture of noninteracting particles, which means its direct identification with the KS single-particle eigenvalues. In Fig. 2 we plot the positions of the t_2 -like KS defect level at the Γ point and at the special point $\mathbf{k} = (2\pi/L)(\frac{1}{4}, \frac{1}{4}, \frac{1}{4})$ as a function of the edge length L of the supercell. The corresponding $E_V(X\text{N})$ for the charge state is used as the energy zero. In the neutral case, the spin-up and spin-down components of the defect level are presented. The spin splitting remains almost constant when one varies the size of the supercell but depends on the nitride. Since no unpaired electrons occur in C_N^{1-} , the spin splitting of the t_2 level is zero in this case. The calculated KS levels are converged for the largest studied supercells with 2744 (BN), 1728 (AlN), and 1000 (GaN) atoms. Perhaps, slight changes may happen for GaN, when the supercell size is further increased. A comparison between the

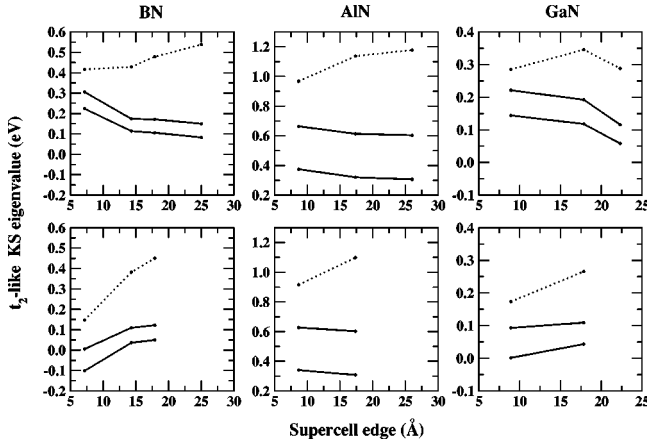


FIG. 2. Position of the t_2 -like KS defect level vs the edge length of the supercell for BN, AlN, and GaN. Fully relaxed and spin-polarized calculations are performed. Upper panels correspond to $\mathbf{k}=(0,0,0)$ (Γ) and lower panels to the special point $\mathbf{k}=(2\pi/L) \times (\frac{1}{4}, \frac{1}{4}, \frac{1}{4})$. The spin-up and spin-down eigenvalues are shown for $\varepsilon_{t_2}(C_N^0)$ (solid lines) and $\varepsilon_{t_2}(C_N^{1-})$ (dotted line). The zero energy is set to the top of valence band $E_V(XN)$.

upper and lower panels shows that the dispersion of the impurity bands indeed becomes smaller with increasing cell size. In InN (not shown in Fig. 2) the KS defect levels of the carbon impurity lie at 30–50 meV in C_N^0 and 90 meV in C_N^{1-} above the VBM.

The converged values for KS defect levels are presented in Table II. They indicate a tendency for a shallow acceptor level of C_N in BN, GaN, and InN, whereas substitutional carbon in AlN should give rise to a deep level in the lower part of the fundamental gap. As a rule, for the negatively charged states the KS eigenvalues lie at higher energies than for the neutral charge state. This is a consequence of the positive Coulomb integrals for the t_2 states. The effective repulsive interaction of the electrons localized at the impurity shifts the single-particle defect level toward higher energies.

In comparison with other works, the results of our calculations exhibit some differences for the positions of the KS defect level, although the carbon impurity in the wurtzite phase is usually considered. In general, previous works did not present the position of t_2 of the negatively charged defect. For c -BN, other calculations including relaxation of the atomic positions predicted a deeper defect level at 0.35–0.50 eV above the VBM (Ref. 21 and 27) than ours, which lies at 0.08–0.15 eV. A deeper defect level at 0.4 eV was also obtained in Ref. 27 for c -GaN, whereas we found it at 0.05–0.12 eV above the VBM for the largest supercells. On the other hand, our results for AlN are in agreement with other calculations^{24,27} which predicted the defect level in the range of 0.3–0.6 eV.

The $(0/1-)$ ionization levels, obtained within the many-body picture by Eq. (3), are shown in Fig. 3 versus the edge length L of the supercell. For the $(0/1-)$ C-acceptor level, converged values with an accuracy better than 50 meV are almost reached for the 2744-, 1728-, and 1000-atom supercells used for BN, AlN, and GaN, respectively. The values of

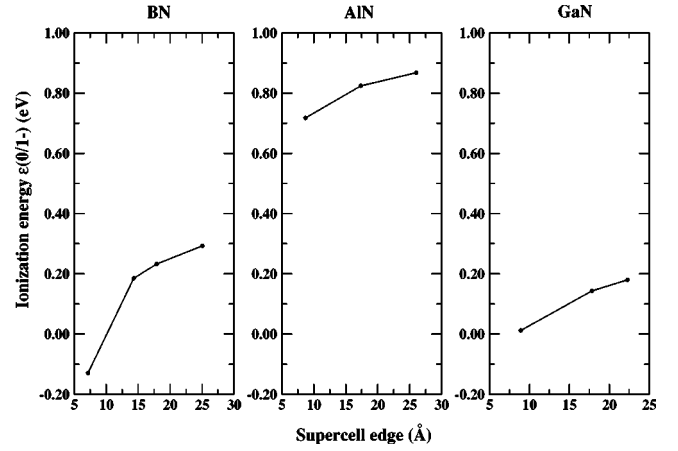


FIG. 3. Ionization level $(0/1-)$ of the carbon acceptor in BN, AlN, and GaN vs the edge length of the supercell.

the $(0/1-)$ ionization levels calculated for the largest supercells are also listed in Table II. They clearly indicate that carbon substitutional on the nitrogen site gives rise to a shallow acceptor for BN, GaN, and InN. Whereas for InN the ionization level $(0/1-)$ is close to the VBM, its value increases along the series InN, GaN, and AlN. As a consequence, carbon in AlN becomes a deep acceptor introducing an energy level of about 0.9 eV above the VBM. Conversely, the acceptor level again becomes shallow in the case of BN. Two reasons could be mentioned to explain this nonmonotonic trend: the strong C-B bonds in the isoelectronic case, which are overestimated within LDA, and the low bond ionicity of BN. In contrast to AlN, GaN, and InN, the bond ionicity of BN is strongly reduced.⁴⁹

There are two other interesting points. First, the activation energy $\varepsilon(0/1-)$ is nearly identical to the corresponding single-particle Kohn-Sham eigenvalue $\varepsilon_{t_2}(q=\frac{1}{2}-)$ according to the transition-state theorem,⁵⁰ and the Janak theorem.⁵¹ A rough estimation of the transition-state value follows from the average of the eigenvalues $\frac{1}{2}[\varepsilon_{t_2}(q=0) + \varepsilon_{t_2}(q=1-)]$ of the partially occupied KS states listed in Table II. For BN, AlN, and GaN the deviations only vary between 3% and 14%. In the case of InN, the trend is still correct, but the absolute value of the activation energy is extremely low. Second, the shallow acceptor levels in BN and GaN can be also described in the framework of the effective-mass theory. One may assume that the supercell edge length $L \approx 3$ nm for the converged results gives an estimate of the Bohr radius of the acceptor r_B of about 1.5 nm. Together with static dielectric constants (ϵ) less than 10, one calculates an effective mass of about $0.3m_0$ ($m = \epsilon\hbar^2/r_B e^2$), i.e., a hole mass with the right order of magnitude. This means that effective-mass states can be described within a supercell approach if the size of the supercell is large enough.

A further indication for the reliability of the calculated defect levels is given by the comparison with experimental data. Both thermal activation energy measurements and PL studies yield to a hole activation energy of the carbon acceptor in c -GaN of about 215 meV.^{8,52} Our calculated value

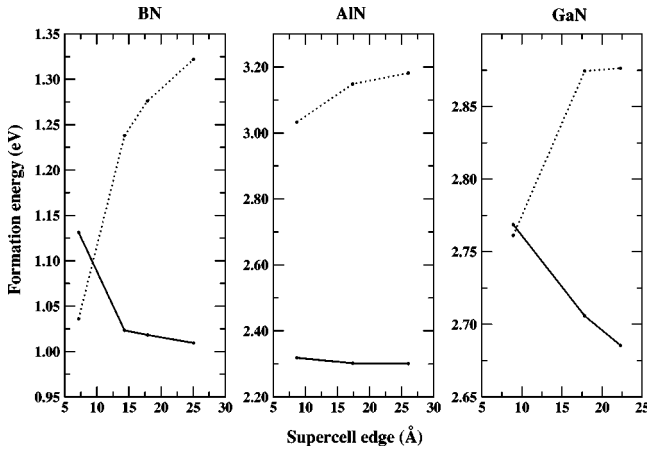


FIG. 4. Formation energy of the carbon impurities C_N^0 (solid line) and C_N^{1-} (dashed line) as a function of the edge length L of the supercell in an XN nitride. The results are presented for simultaneous C-rich and X-rich preparation conditions. A p -type doping ($\varepsilon_F=0$) is assumed for $q=1-$. The results refer to supercells with $(2n)^3$ atoms with $n=2, 4, 5,$ and 7 (BN), $n=2, 4,$ and 6 (AlN), and $n=2, 4,$ and 5 (GaN).

$\varepsilon(0/1-)=182$ meV underestimates slightly the measured one. However, according to Fig. 2 one may expect that in a more converged calculation, the theoretical value will approach better the measured energy. The agreement of the activation energies measured by different methods is somewhat surprising. For the optical hole activation energy, $\varepsilon_E(0/1-)=\varepsilon(0/1-)+\Delta E_{FC}^{thermal}$, measured in a PL experiment, one finds a value that is enlarged by the thermal Franck-Condon shift $\Delta E_{FC}^{thermal}=89$ meV. However, one has to consider the exciton binding energy, which reduces the value of the optical hole activation energy. From free excitons we know that typical binding energies are not much smaller than $\Delta E_{FC}^{thermal}$.⁵³ The resulting compensation may explain why in thermal activation and PL experiments^{8,10,52} nearly the same energies have been observed.

C. Energetics of the acceptor formation

The convergence of the formation energy Ω_f [Eq. (1)] is shown in Fig. 4 with respect to the supercell size for BN, AlN, and GaN and for the most important preparation condition, i.e., simultaneous carbon-rich and cation-rich condition. For $q=1-$ the doping level is fixed at $\varepsilon_F=0$ (p -type doping). Calculations using 32-atom supercells may not give even a quantitative result for single impurities, since one considers in reality an alloy with an impurity concentration equal to 6.25%. Figure 4 indicates that the largest supercells under consideration can be used safely to derive the defect formation energy at least for $q=0$. The only exception could be GaN for which even larger supercells may be needed. The absolute variations of this quantity of about 0.1 eV are similar for the carbon acceptor in the three nitrides considered. In the limit of convergence, one finds that, under the chosen conditions, the formation energy of the neutral impurity is favored in comparison to the negatively-charged one. For BN and GaN with an effective-mass-like acceptor, the treat-

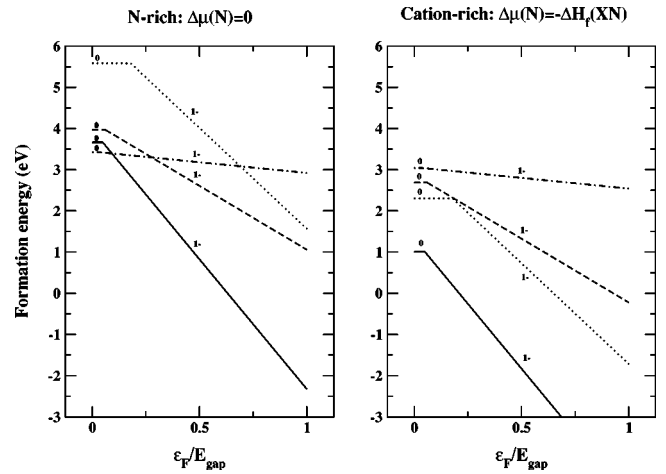


FIG. 5. Formation energies of the C acceptor for the neutral and negatively charged states in BN (solid line), AlN (dotted line), GaN (dashed line), and InN (dot-dashed line) as a function of the electron chemical potential. Results are obtained for 2744-, 1728-, 1000-, and 512-atom supercells, respectively. C-rich preparation conditions are assumed simultaneously with N-rich (left panel) and cation-rich (right panel).

ment within small supercells fails. One obtains similar values for the formation energies in both $q=0$ and $1-$ or even lower formation energies for $q=1-$. Conversely, the formation energies of the deep acceptor in AlN are only slightly sensitive to the supercell size on the energy scale of the formation energies. The formation energy for the carbon impurity increases with respect to the cation atomic number of the host material, reaching about 3.0 eV for InN in 512-atom supercells. For the most converged calculations the formation energy of the negatively-charged defect is always higher than for the neutral state under the chosen preparation conditions. The difference between the two energies is proportional to the hole activation energy.

A study about the influence of the preparation conditions and doping level on the formation energies of C_N^q is presented in Fig. 5 for the largest supercells considered. Again, only the C-rich preparation conditions are considered and the reduced Fermi level ε_F varies between zero and the quasiparticle fundamental gap of the compound XN . The knee points separating the two charged states in Fig. 5 give exactly the ionization levels shown in Table II, and lie at 5%, 18%, 6%, and 4% of the quasiparticle fundamental gap, respectively, for BN, AlN, GaN, and InN. As expected, the cation-rich conditions favor the formation of an isolated carbon impurity substitutional to a nitrogen site and the single negatively charged state is more likely to occur than the neutral carbon under n -type preparation conditions. The negatively charged carbon presents lower formation energies than the neutral one for the majority of the doping levels. Under cation-rich preparation conditions, the formation energies show a clear trend with the atomic number of the cation in the group-III nitride. In this case the higher the atomic number the higher is the formation energy. For N-rich conditions this trend changes and one finds that the formation energy increases along the series BN, GaN, and AlN. The formation

energy of C_N^q in InN shows a behavior distinct from the other nitrides lying in the range 2.5–3.5 eV, rather independent of doping level or preparation conditions.

Formally the results in Fig. 5 indicate that a C-doped BN crystal would be unstable in the presence of free electrons in the system. The figure shows negative formation energies under high- n -type doping conditions. The excess of electrons in the system stabilizes the carbon impurity in its negatively-charged state and as a result strong C-B bonds are formed around it. The corresponding binding energies are probably overestimated by the DFT-LDA treatment. In addition, the quasiparticle fundamental energy gap, used to limit the variation of ε_F , is wider than the DFT-LDA ones, which shifts automatically the formation energies for negatively-charged states to lower values.

In contrast to our results, Orellana and Chacham²¹ calculated negative formation energies for both neutral and negatively charged states of the carbon impurity in c -BN. In comparison with the results reported by Gorczyca *et al.*²⁷ for C_N^0 in the cubic phase, we obtain lower formation energies for BN, higher formation energies for AlN and similar results for GaN. For w -GaN, Bogusławski and co-workers^{23,24} calculated almost the same formation energy of 1.6 eV for $q=1+$, $q=0$, and $q=1-$, a value which is lower than ours. The same authors found that only the positively-charged defect would be stable in w -AlN.

IV. SUMMARY

We have presented *ab initio* calculations of the neutral (C_N^0) and the negatively charged (C_N^{1-}) carbon substitutional impurity in the group-III nitrides. Total-energy calculations within the framework of a plane-wave-pseudopotential code have been performed taking the lattice relaxation and spin polarization into account. Because of the shallow character of the carbon acceptor in BN, GaN, and InN, special care is taken in the supercell approach. The convergence of the de-

fect properties with respect to the edge length of the supercell is studied in detail. As a consequence, extremely large supercells with 2744 (BN), 1728 (AlN), 1000 (GaN), and 512 (InN) atoms have been used to model an isolated defect. Despite the small size of B, C, and N cores as well as of the cores of Ga and In below the d shells, the treatment of so many electrons and so large supercells was possible due to the use of supersoftened non-normconserving pseudopotentials.

Independent of the nitride and the charge state of the defect, a breathing-mode relaxation occurs around the carbon impurity. Substitutionally to the nitrogen site carbon gives rise to an acceptor level. The corresponding hole activation energy $\varepsilon(0/1-)$ increases along the series InN, GaN, and AlN. As a consequence, the acceptor level in AlN is shifted by about 0.9 eV toward the middle of the fundamental gap, which characterizes C_N as a deep acceptor in AlN. In BN C_N also forms a shallow acceptor. We trace the resulting non-monotonical chemical trend along InN, GaN, AlN, and BN back to the interplay of opposite effects, the low bond ionicity in BN, and the extremely strong B-C bonds. The formation energies are low in all the nitrides, in such a way that the incorporation of carbon in the N sublattice should be likely, even in presence of a p -type background doping. The calculated values of the hole activation energy are comparable to energies extracted from thermal and optical measurements in c -GaN. The experimental observation of nearly the same activation energies in Hall experiments and photoluminescence is explained by compensation effects due to the different lattice relaxations and electron-hole binding.

ACKNOWLEDGMENTS

This work was supported by the Deutsche Forschungsgemeinschaft in the framework of the central project “Group-III nitrides and their heterostructures: Growth, basic properties and applications” (Grant No. Be 1346/8-5) and FAPESP, a Brazilian funding agency.

¹O. Ambacher, J. Phys. D **31**, 2653 (1998).

²S. Fischer, C. Wetzels, E.E. Haller, and B.K. Meyer, Appl. Phys. Lett. **67**, 1298 (1995).

³G.-C. Yi and B.W. Wessels, Appl. Phys. Lett. **70**, 357 (1997).

⁴X. Tang, F. Hossain, K. Wongchotigul, and M.G. Spencer, Appl. Phys. Lett. **72**, 1501 (1998).

⁵P. Widmayer, H.-G. Boyen, P. Ziemann, P. Reinke, and P. Oelhafen, Phys. Rev. B **59**, 5233 (1999).

⁶M.P. Thompson, G.W. Auner, T.S. Zheleva, K.A. Jones, S.J. Simko, and J.N. Hilfiker, J. Appl. Phys. **89**, 3331 (2001).

⁷J. Neugebauer and C.G. Van de Walle, Adv. Solid State Phys. **35**, 25 (1996).

⁸D.J. As, Phys. Status Solidi B **210**, 445 (1998); D.J. As, T. Simonsmeier, J. Busch, B. Schöttker, M. Lübbers, J. Mimkes, D. Schikora, K. Lischka, W. Kriegseis, W. Burkhardt, and B.K. Meyer, MRS Internet J. Nitride Semicond. Res. **4S1**, G3.24 (1999).

⁹C.R. Abernathy, J.D. Mackenzie, and S.J. Pearton, Appl. Phys. Lett. **66**, 1969 (1995).

¹⁰D.J. As and U. Köhler, J. Phys.: Condens. Matter **13**, 8923 (2001).

¹¹U. Birkle, M. Fehrer, V. Kirchner, S. Einfeldt, D. Hommel, S. Strauf, P. Michler, and J. Gutowski, MRS Internet J. Nitride Semicond. Res. **4S1**, G5.6 (1999).

¹²*Properties of group-III nitrides*, edited by J.H. Edgar (INSPEC, London, 1994).

¹³H. Okumura, H. Hamaguchi, K. Ohta, G. Feuillet, K. Balakrishnan, Y. Ishida, S. Chichibu, H. Nakanishi, T. Nagatomo, and S. Yoshida, Mater. Sci. Forum **264**, 1167 (1998).

¹⁴R.H. Wentorf, J. Chem. Phys. **26**, 956 (1957).

¹⁵M. Lu, A. Bousetta, R. Sukach, A. Bensaoula, K. Walters, K. Eipers-Smith, and A. Schultz, Appl. Phys. Lett. **64**, 1514 (1994).

¹⁶I. Petrov, E. Mojab, R.C. Powell, J.E. Greene, L. Hultman, and J.-E. Sundgren, Appl. Phys. Lett. **60**, 2491 (1992).

- ¹⁷R.C. Powell, N.-E. Lee, Y.-W. Kim, and J.E. Greene, *J. Appl. Phys.* **73**, 189 (1993).
- ¹⁸A.P. Lima, A. Tabata, J.R. Leite, S. Kaiser, D. Schikora, B. Schöttker, T. Frey, D.J. As, and K. Lischka, *J. Cryst. Growth* **201-202**, 396 (1999); A. Tabata, A.P. Lima, L.K. Teles, L.M.R. Scolfaro, J.R. Leite, V. Lemos, B. Schöttker, T. Frey, D. Schikora, and K. Lischka, *Appl. Phys. Lett.* **74**, 362 (1999).
- ¹⁹V.A. Gubanov, L.A. Hemstreet, C.Y. Fong, and B.M. Klein, *Appl. Phys. Lett.* **69**, 227 (1996).
- ²⁰M. Marques, L.E. Ramos, L.M.R. Scolfaro, L.K. Teles, and J.R. Leite, in *Proceedings of the 25th International Conference on the Physics of Semiconductors*, Osaka 2000, edited by N. Miura and T. Ando (Springer-Verlag, Berlin, 2001), p. 1411.
- ²¹W. Orellana and H. Chacham, *Phys. Rev. B* **62**, 10 135 (2000).
- ²²D.W. Jenkins and J.D. Dow, *Phys. Rev. B* **39**, 3317 (1989).
- ²³P. Boguslawski, E.L. Briggs, and J. Bernholc, *Appl. Phys. Lett.* **69**, 233 (1996).
- ²⁴P. Boguslawski and J. Bernholc, *Phys. Rev. B* **56**, 9496 (1997).
- ²⁵I. Gorczyca, A. Svane, and N.E. Christensen, *Solid State Commun.* **101**, 747 (1997).
- ²⁶I. Gorczyca, A. Svane, and N.E. Christensen, *MRS Internet J. Nitride Semicond. Res.* **2**, 18 (1997).
- ²⁷I. Gorczyca, A. Svane, and N.E. Christensen, *Phys. Rev. B* **60**, 8147 (1999).
- ²⁸L.E. Ramos, L.K. Teles, L.M.R. Scolfaro, J.L.P. Castineira, A.L. Rosa, and J.R. Leite, *Phys. Rev. B* **63**, 165210 (2001).
- ²⁹C. Stampfl, C.G. Van de Walle, D. Vogel, P. Krüger, and J. Pollmann, *Phys. Rev. B* **61**, 7846 (2000).
- ³⁰G. Makov and M.C. Payne, *Phys. Rev. B* **51**, 4014 (1995).
- ³¹L.N. Kantorovich, *Phys. Rev. B* **60**, 15 476 (1999); L.N. Kantorovich and I.I. Tupitsyn, *J. Phys.: Condens. Matter* **11**, 6159 (1999).
- ³²P. Hohenberg and W. Kohn, *Phys. Rev.* **136**, B864 (1964).
- ³³W. Kohn and L.J. Sham, *Phys. Rev.* **140**, A1139 (1965).
- ³⁴J.P. Perdew and A. Zunger, *Phys. Rev. B* **23**, 5048 (1981).
- ³⁵U. von Barth and L. Hedin, *J. Phys. C* **5**, 1629 (1972).
- ³⁶J. Furthmüller, P. Käckell, F. Bechstedt, and G. Kresse, *Phys. Rev. B* **61**, 4576 (2000).
- ³⁷G. Kresse and J. Furthmüller, *Comput. Mater. Sci.* **6**, 15 (1996); *Phys. Rev. B* **54**, 11 169 (1996).
- ³⁸R.P. Feynman, *Phys. Rev.* **56**, 340 (1939).
- ³⁹H.J. Monkhorst and J.D. Pack, *Phys. Rev. B* **13**, 5188 (1976).
- ⁴⁰K. Laasonen, R.M. Nieminen, and M.J. Puska, *Phys. Rev. B* **45**, 4122 (1992).
- ⁴¹S.B. Zhang and J.E. Northrup, *Phys. Rev. Lett.* **67**, 2339 (1991).
- ⁴²M.P. Surh, S.G. Louie, and M.L. Cohen, *Phys. Rev. B* **43**, 9126 (1991).
- ⁴³A. Rubio, J.L. Corkill, M.L. Cohen, E.L. Shirley, and S.G. Louie, *Phys. Rev. B* **48**, 11 810 (1993).
- ⁴⁴V.Y. Davydov, A.A. Klochikhin, R.P. Seisyan, V.V. Emtsev, S.V. Ivanov, F. Bechstedt, J. Furthmüller, H. Harima, A.V. Mudriy, J. Aderhold, O. Semchinova, and J. Graul, *Phys. Status Solidi B* **229**, R1 (2002).
- ⁴⁵C.G. Van de Walle, D.B. Laks, G.F. Neumark, and S.T. Pantelides, *Phys. Rev. B* **47**, 9425 (1993).
- ⁴⁶U. Grossner, J. Furthmüller, and F. Bechstedt, *Appl. Phys. Lett.* **74**, 3851 (1999).
- ⁴⁷J.I. Pankove, *Optical Processes in Semiconductors* (Dover, New York, 1971).
- ⁴⁸L.K. Teles, L.M.R. Scolfaro, J.R. Leite, L.E. Ramos, A. Tabata, J.L.P. Castineira, and D.J. As, *Phys. Status Solidi B* **216**, 541 (1999).
- ⁴⁹U. Grossner, J. Furthmüller, and F. Bechstedt, *Phys. Rev. B* **58**, R1722 (1998).
- ⁵⁰J.C. Slater, *Adv. Quantum Chem.* **6**, 1 (1972).
- ⁵¹J.F. Janak, *Phys. Rev. B* **18**, 7165 (1978).
- ⁵²U. Köhler, M. Lübbbers, J. Mimkes, and D.J. As, *Physica B* **308-310**, 126 (2001).
- ⁵³B. Monemar, *Phys. Rev. B* **10**, 676 (1974).